Cement & Concrete Composites 40 (2013) 7–13

Contents lists available at SciVerse ScienceDirect

Cement & Concrete Composites

journal homepage: www.elsevier.com/locate/cemconcomp

Development of alkali activated cement from mechanically activated silico-manganese (SiMn) slag

Sanjay Kumar [a,*], P. García-Triñanes [b], Amândio Teixeira-Pinto [c], M. Bao [b]

[a] CSIR – National Metallurgical Laboratory, Jamshedpur 831 007, India
[b] School of Engineering, Chemical Engineering Department, University of Santiago de Compostela, 15705 Santiago de Compostela, Spain
[c] Universidade Privada de Angola, Caixa Postal 888, Lubango, Angola

ARTICLE INFO

Article history:
Received 19 October 2012
Received in revised form 22 March 2013
Accepted 24 March 2013
Available online 6 April 2013

Keywords:
Alkaline activation
SiMn slag
Reaction kinetics
Microstructure
Properties

ABSTRACT

Silico-manganese (SiMn) slag has been used to develop alkali activated cement binder. The reactivity of SiMn slag was altered by mechanical activation using eccentric vibratory and attrition mill. The reaction kinetics during alkali activation of SiMn slag and structural reorganization were studied using isothermal conduction calorimetry and Fourier transform infrared spectroscopy. The particle size after milling was smaller in attrition milled samples but reaction started earlier in vibratory milled samples due to more reactivity. This observation was further supported by compressive strength which was highest in samples prepared from vibratory milled slag. The main reaction product was C–S–H (C = CaO, S = SiO_2, H = H_2O) of low crystallinity of different types with varying Si/Al and Ca/Si ratio. An attempt has been made to relate the microstructure with mechanical properties. The results obtained in this study establish technical suitability of SiMn slag as raw material for alkali activated cement.

1. Introduction

Silicomanganese (SiMn) slag is a by-product generated during production of silico-manganese alloy by carbothermic reduction of raw materials in submerged electric arc furnace. The global production of silico-manganese alloy in year 2009 was ~7.4 million metric tons [1]. Typically the slag generation is about 1.2–1.4 tons for every ton of SiMn alloy produced thus the slag generated is in the tune of 8.9–10.4 million tons per annum. Only a limited quantity of these slag are used for land filling. The remaining slag is getting accumulated for a long period and thus the total global inventory of SiMn slag is much higher. SiMn slag consists of oxides like SiO_2, CaO, Al_2O_3 and MgO and is mostly glassy in nature. The chemistry of SiMn slag is similar to blast furnace slag but has higher MnO content. Thus the majority of the research on the use of SiMn slag is directed towards its chemical suitability and technical viability in blended cement [2–4]. Typically in SiMn slag, the main constituents SiO_2, CaO and Al_2O_3 comprise more than 70% of the total composition. Thus it can be considered as potential raw material for alkali activated binders [5].

Alkali-activated binders are a class of materials with similar properties to hydraulic binders that are formed due to reaction between an alkaline activator with solid pozzolanic or cementitious aluminosilicate powder [6]. The development of alkali activated binders was first reported in 1940s [6,7]. Because of its low environment impact than Portland cement, good durability and possibility of using varieties of industrial waste, it has become a material of interest. Many developments have taken place on alkali activated binders starting from chemistry to the reaction mechanism and characterization of civil engineering applications [8–13]. Granulated blast furnace slag (GBFS), a by-product of iron making process, has been the most widely studied material for their use in alkali-activated binders [9]. The dominant binder phases of these systems are generally identified to be calcium silicate hydrate (C–S–H) which is relatively low in Ca [10]. The chemical composition of SiMn slag is close to GBFS, thus the present study has been planned to explore its suitability for alkali activated binders. Limited information was available on use of SiMn slags so probing studies were carried out in the beginning to know its behavior with an alkali solution. The strength development and setting time was much slower as compared to GBFS of the same fineness. This might be due to slow reactivity of SiMn slag. Thus it was decided to enhance the reactivity using mechanical activation. The merit of using mechanical activation (MA) for improving bulk and surface reactivity is well accepted [14–16]. MA offers the possibility to alter the reactivity of solids through physicochemical

* Corresponding author. Address: Principal Scientist & Group Leader, Recycling & Waste Utilization, CSIR – National Metallurgical Laboratory, Jamshedpur 831 007, India. Tel.: +91 657 2345049, +91 9939326346 (Mobile); fax: +91 657 2345213.
E-mail addresses: sanjay_kumar_nml@yahoo.com, sunju@nmlindia.org (S. Kumar).

0958-9465/$ - see front matter © 2013 Elsevier Ltd. All rights reserved.
http://dx.doi.org/10.1016/j.cemconcomp.2013.03.026

changes in bulk and surface without altering the overall chemistry of the material [14–16]. Some very interesting finding on the MA of blast furnace slag and fly ash has been recently reported by some of us and other researchers [17–20]. Complete hydration was achieved for mechanically activated slag without any chemical addition [21]. Mechanical induced reactivity of fly ash has been exploited to tailor properties of alkaline activated products, with compressive strength results of up to 120 MPa that can be produced through judicious application of MA along with other processing parameters [17,22] .

The objective of the present investigation was to carry out a systematic study on the alkaline activation behavior of SiMn slag with different levels of reactivity to be shown by calorimetry analysis. The reactivity of SiMn slag was altered using different milling devices such as ball mill, attrition mill and eccentric vibratory mill. The effect of milling and mechanical activation on reaction, structure and properties was elucidated using isothermal conduction calorimetry, Fourier transform infrared spectroscopy (FTIR), X-ray diffractometry (XRD), scanning electron microscopy (SEM) and by evaluation of mechanical properties. An attempt has been made to correlate the reaction with structure and properties.

2. Materials and methods

The SiMn slag used in this study was obtained from FERROATLÁNTICA S.L. (Spain), a leading global producer of manganese ferroalloys. The chemical analysis of the slag was carried out using X-ray fluorescence (XRF). Table 1 shows that the main constituents of slag are SiO_2, CaO and Al_2O_3 and comprised ~80% of the total composition. The slag also contains MnO and MgO in significant account.

Fig. 1 shows the XRD diffraction pattern of SiMn slag. The main feature of the XRD was a diffused wide band that extended from 20° to 40° and localizing at approximately 30° 2θ. This diffused band is characteristic of glassy phase. The mineral composition of glassy phase is mainly composed of Akermanite ($Ca_2Mg(Si_2O_7)$), Wollastonite ($CaSiO_3$), Diopside ($MgCaSi_2O_6$) and Quartz (SiO_2). A semi quantitative analysis using Rietveld Method using SIROQUANT software indicated the following phase composition: Akermanite 32.2%, Wollastonite 20.6%, Diopside 36.2% and Quartz 10.8%.

The as received slag was in lump form. The slag lump was first crushed using Lab scale Jaw Crusher (AIMIL, India). The crushed material was subjected to normal milling using ball mill and mechanical activation using attrition and eccentric vibration mill, using the parameters given in Table 2. Ball milling was done for 1 h in a laboratory ball mill (AIMIL, India). Attrition milling was carried out using a batch type wet attrition mill (Model PE-075, NETZSCH Feinmahltechnik GmbH, Selb, Germany). The material was milled for 10 min in de-ionized water and then dried. The rationale of using water as milling medium is we observed in our previous work on the attrition milling of GBFS [19] that hydration does not start during milling for 10–15 min in water. As the reactivity of SiMn slag is lower than GBFS, it was assumed that hydration has not started during milling. Vibration milling was carried out in the eccentric vibratory mill (SIEBTECHNIK, ESM 234, Germany) for 30 min. The 10 min and 30 min milling time in attrition and vibration mill respectively were used to obtain particle size distribution with X_{50} value close to 5 μm.

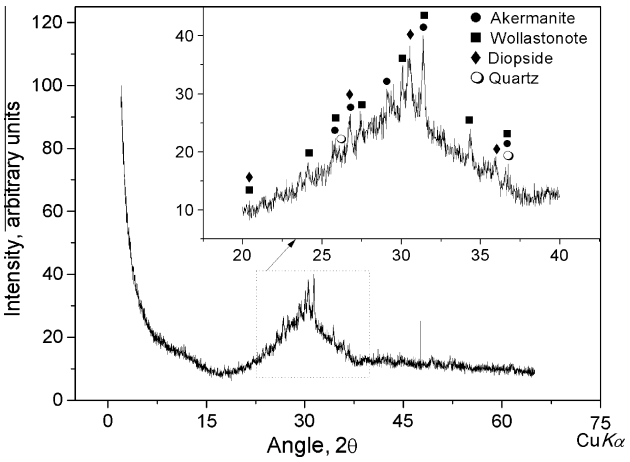

Fig. 1. X-ray diffraction pattern of SiMn slag. The area between 20° and 40° is shown at higher magnification in the inside box.

Particle size analysis of the milled slag was carried out using a laser particle size analyzer (MASTERSIZER S, Malvern, UK). The specific surface area was measured using MICROMERITICS (USA) specific surface area analyzer (Model ASAP2020). To monitor the progress of reactions isothermal conduction calorimetry was carried out at 27 °C. The rationale for using 27 °C considers the accepted ambient temperature of cementitious material as per BIS specification [23]. The rate of heat evolution during the reaction (dq/dt) was measured using an eight channel isothermal conduction calorimeter (TAM AIR, Thermometric AB, Jarafalla, Sweden). Analytical grade sodium hydroxide pellets (98% purity) was used to prepare the activator solution. An alkaline activator of 6 M concentration was prepared in distilled water at least 24 h before use. 7 g solid sample and 3.5 ml of activator solution were used throughout the study. Calorimetric studies were carried out at 27 °C. The results obtained were presented in offset mode. Fourier Transform Infrared Spectroscopy ((FT-IR-410 JASCO, USA) was used for structural characterization of activated products. IR samples were prepared by mixing with KBr, as usual. XRD patterns were recorded on a SIEMENS X-ray diffractometer (Model D500), using Co K_α radiation with a Fe-filter. The scanning speed of 1°/min was used and the samples were scanned from 10° to 60° 2θ angle. Morphological characterization of the fractured samples was done by a scanning electron microscope (JEOL SEM 840A) fitted with a Kevex Energy Dispersive Spectrometer (EDS) for X-ray micro-analysis after carbon coating on the fractured surface. The X-ray micro-analysis of areas of interest was determined from the average of ten analyses and used to calculate elemental ratios.

For setting time and compressive strength determination, the liquid (alkali solution) to solid ratio was kept 0.35. The samples were prepared at 27 ± 2 °C and under relative humidity of 65%. The initial and final setting time was determined by using Vicat Apparatus (AIMIL, India) on a homogeneous paste prepared by thoroughly mixing slag powder and alkali solution. For compressive strength $7 \times 7 \times 7$ cm^3 samples were prepared by vibro-casting of the paste. Samples were cured for 7 and 28 days in a closed container at 27 ± 2 °C. Compressive strength was tested on an Automatic Compression Testing Machine (AIMIL COMPTEST 2000, India).

Table 1
Chemical composition of SiMn slag.

Oxides	SiO_2	Al_2O_3	CaO	Fe_2O_3	MgO	MnO	Na_2O	K_2O	TiO_2	SO_3
Percent	42.6	12.2	25.2	1.0	4.2	9.9	0.36	2.2	0.36	0.12

Table 2
Milling parameters.

Milling type	Ball milling (BM)	Attrition milling (AM)	Eccentric vibratory milling (VM)
Feed material	Pulverized	Pulverized and ball milled for 15 min	Pulverized and ball milled for 15 min
Medium	Dry	Wet	Dry
Milling time, Min	60	15	30
Ball to material ratio	1:10	1:10	1:20
RPM	40	1500	Vibration
Processing after milling	None	Drying and powdering	None

3. Results and discussion

3.1. Mechanical activation of SiMn slag and its reactivity

Attrition mills, also known as stirred ball mills, agitator bead mills or agitator mills have emerged as efficient milling devices for fine grinding and production of narrow size distribution of the milled products [24–27]. The high efficiency of these mills results due to smaller size (2 mm to < 0.5 mm) grinding media and high agitator speed (may go up to a few thousand RPM). While the small size of media provides a larger contact surface between the media and material being ground (high stress number), higher agitator speed gives rise to greater kinetic energy of the media (stress intensity) [27]. Eccentric vibratory mill (EVM) due to the eccentric drive generates 5-axis elliptical, circular and linear vibrations. This results in a very significant intensification of the impact force/ milling energy leading to efficient milling and mechanical activation [28,29]. The particle size analysis of SiMn slag after different types of milling is given in Fig. 2. Attrition mill (AM) samples show finest and narrow particle size distribution followed by Vibratory milling (VM) and Ball milling (BM) respectively.

To get an idea about the reactivity of BM, VM and AM, all three samples were mixed with equal quantity of NaOH (6 M) solution and kept in the beaker (Fig. 3a). BM samples settled completely in 30 min whereas the VM and AM samples formed stable suspensions. The faster settling behavior can be attributed to coarse particle size of BM. BM samples have taken ~48 h for complete hardening whereas for samples AM and VM, complete hardening was achieved within 4 h. Formation of carbonate on the surface

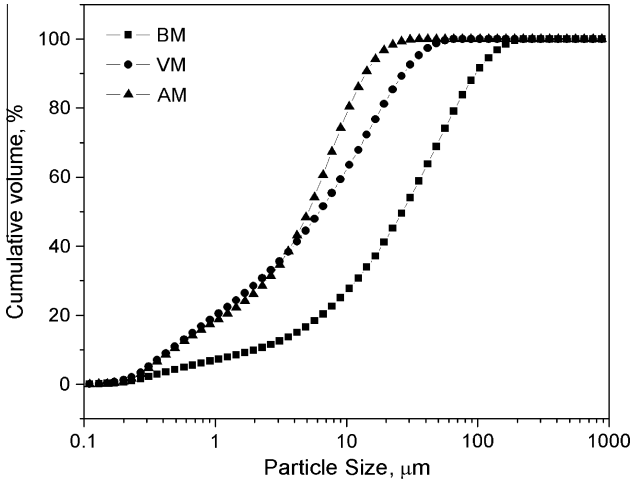

Fig. 2. Particle size analysis of BM, VM and AM samples.

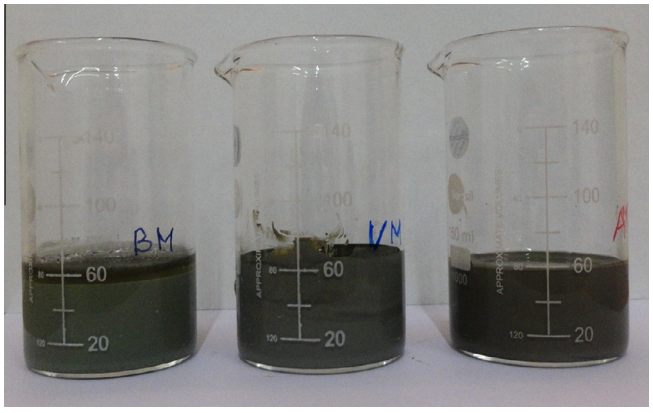

Fig. 3a. VM and AM with alkali solution shows stable suspension whereas BM shows settling behavior.

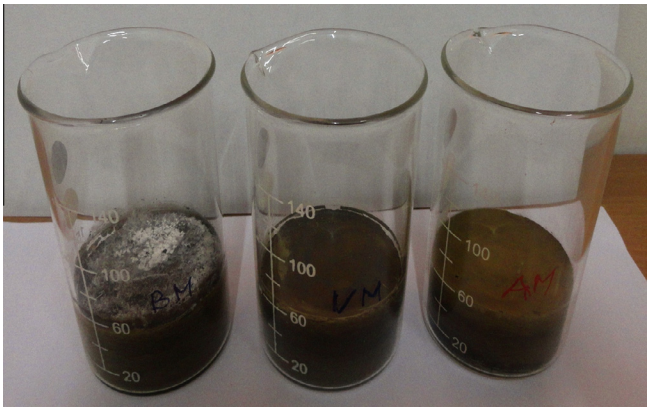

Fig. 3b. Samples of alkali activated BM shows formation of carbonate layer on the exposed surface.

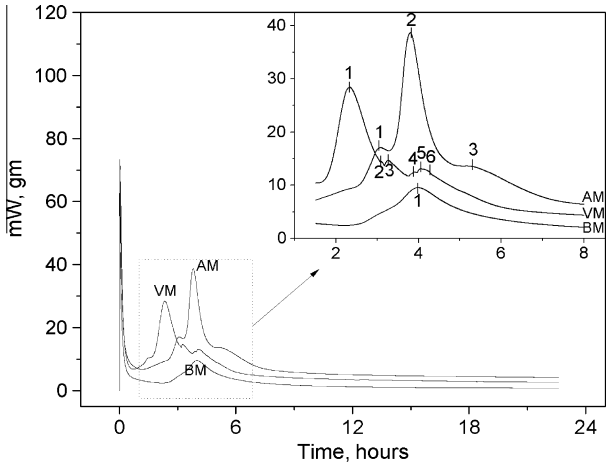

Fig. 4. Calorimetric curve of BM, VM and AM samples. The region between 2 and 8 h is shown at higher magnification in the inside box.

Table 3
Peak characteristic of SiMn slag under alkali activation.

Sample	Peak no.	Peak start, min	Peak end, min	Peak area, integrated	Remarks
BM	1	144	392	49,057	Precipitation of C–S–H
AM	1	85	197	29,689	Precipitation of C–S–H
	2	197	304	102,706	Precipitation of C–S–H
	3	304	463	39,445	Restructuring
VM	1	54	185	76,588	Precipitation of C–S–H
	2	185	191	2648	–
	3	191	225	14,622	Precipitation of C–S–H
	4	225	238	4510	–
	5	238	246	3424	Hydrotalcite type gel
	6	246	372	23,009	Restructuring

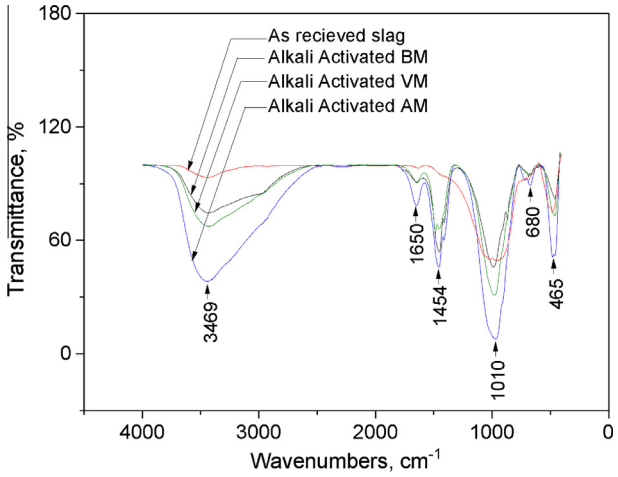

Fig. 5. FTIR spectra of alkali activated samples of BM, VM and AM.

of BM samples was due to un-reacted alkalies which formed carbonate in contact with air (Fig. 3b).

3.2. Isothermal conduction calorimetry studies

Fig. 4 shows the heat evolution curve obtained by isothermal conduction calorimetry of the samples at 27 °C for 24 h. The first peak which looks like a straight line in the beginning can be assigned to pre-induction stage. Irrespective of sample behavior, the occurrence of this peak at the same point in all samples, this phenomenon was attributed to physical process such as wetting of particles and initial dissolution and not to a chemical process [30]. As mixing was carried out outside the instrument and the mixed pastes were then introduced into the calorimeter; time zero on the plots represent the time at which the sample was placed in the instrument, which was ~2 min after the start of mixing in each case. An induction period before beginning of second peak which can be assigned to gelation process was observed in all the cases [30]. In BM sample, only one broad peak observed with a shoulder at 195 min. This shoulder has been transformed into a peak (peak 1) in AM sample. In AM and VM samples, three and six peaks were identified respectively. The nature of the peak of BM was similar to the peak obtained in calorimetric studies of alkali activated blast furnace slag and attributed to precipitation of C–S–H gel [10]. In VM and AM samples, the main reaction peak i.e. peaks 1 and 2 respectively can be ascribed to precipitation of C–S–H gel [10]. In VM, the minor peak occurring after main reaction peak can be attributed to hydrotalcite [10] and Mn rich gel, which formed at an early age due to increased reactivity. The peak characteristic such as starting time, ending time and area under the peak of

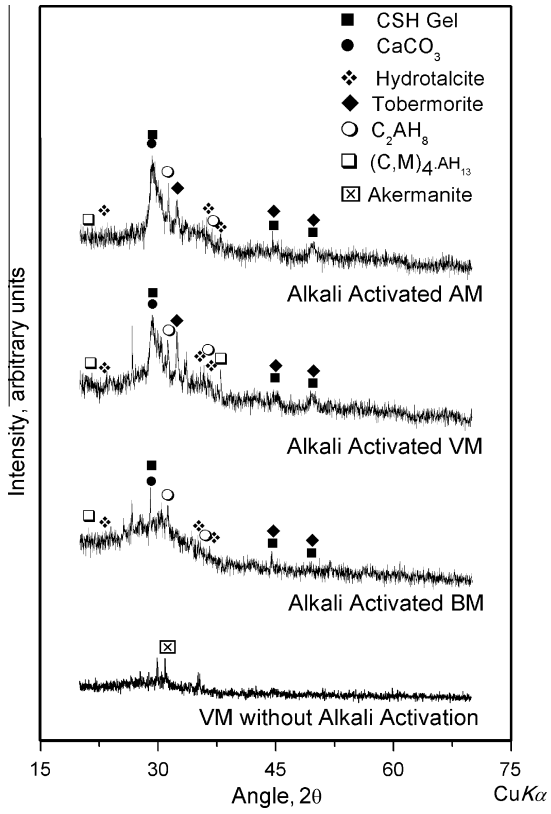

Fig. 6. X-ray diffraction pattern of activated samples of BM, VM and AM.

BM, AM and VM samples were identified by deconvolution using MICROCAL ORIGIN 8 software and are shown in Table 3.

3.3. FTIR

Fig. 5 shows the FT-IR spectra of alkali activated BM, VM and AM. FT-IR spectra of as received slag has also been incorporated to understand the change in spectra due to alkali activation. In all spectra, the positions of the absorption bands were nearly similar but relative intensities were more intense in VM and AM. A broad band at ~3469 and a weak peak at ~1650 $cm^{-1}$was due to the stretching vibrations of O—H bonds and H—O—H bending vibrations of interlayer adsorbed H_2O molecule, respectively [31]. These bands were insignificant in as received slag, indicating that these were formed due to alkali activation. Increased intensity in AM and VM can be ascribed to the adsorption of more molecules of H_2O. The absorption bands at ~1454 cm^{-1} is due to stretching vibrations of C═O, C — O confirming the presence of carbonate

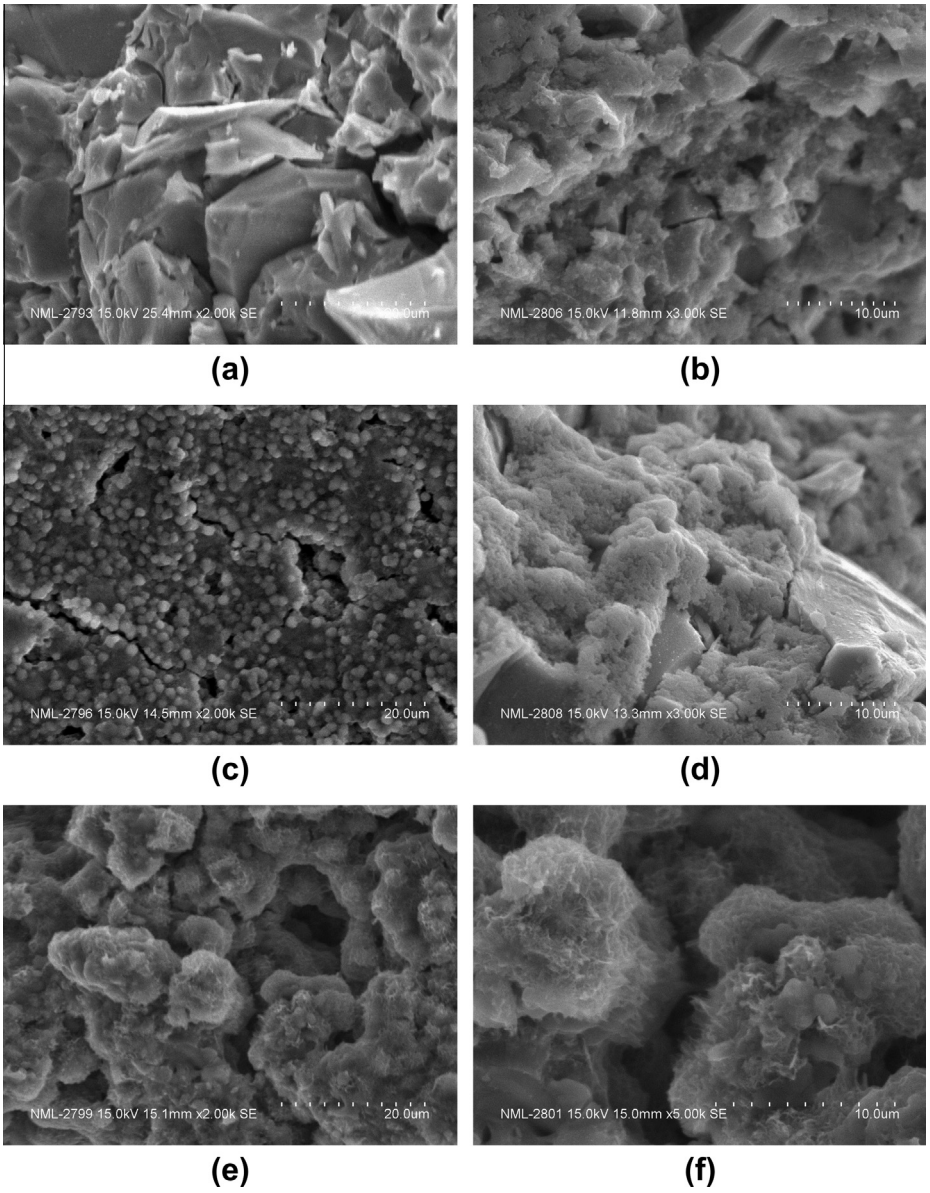

Fig. 7. Scanning electron micrograph of alkali activated samples (a) BM sample comprised of discrete particles of slag, (b) gel phase in AM sample, (c) globules type structure in VM sample, (d) dense gel structure in VM sample, and (e and f) honeycomb type gel.

Table 4
Summary of microstructural features obtained using SEM–EDS.

Sample name	Features	EDS summary, molar ratio	Remarks
BM	Mostly un-reacted slag	Ca/Si = 2.5–3	
AM	Partially reacted slag particles, densely packed	Ca/Si = 2–2.8	C–S–H gel with Na in structure
	Gel phase	Ca/Si = 1.1–1.6, Si/Al = 1.9–2.8	Calcium silicate hydrate (C–S–H gel type I) rich in Al with Mn in structure
VM	Globular grains of 5–10 μm size	Ca/Si = 2.0–2.6, Ca/Mn = 1.2–1.8	Mn rich gel with composition close to hydrotalcite
	Dense gel phase 1	Ca/Si = 0.8–1.6, Ca/Mn = 2.1–2	Calcium silicate hydrate (C–S–H gel type I) with Mn in structure
	Dense gel phase 2 (honeycomb type)	Ca/Si = 1.4–3.0, Ca/Mn = 1.9–2.5	Calcium silicate hydrate (C–S–H gel type II) with Mn in structure

groups [32,33]. Characteristic bands corresponding to Si—O vibration were detected at ~1010 cm^{-1}. In as received slag a broad band with two minor peaks was observed in this region. These peaks were sharp and intense in alkali activated samples showing prominent Si—O vibration. Peaks at ~680 and ~465 cm^{-1} are due to bending vibration of Si—O—Al and stretching vibrations of Fe—O bonds respectively [34,35]. Increased intensities in the case of AM and VM confirmed the enhanced dissolution of silicate minerals.

Table 5
Physical properties of SiMn slag based products.

	Setting time, min		Compressive strength, MPa	
	Initial	Final	3 day	28 day
BM	390	472	6	24
AM	67	105	26	66
VM	57	90	42	101

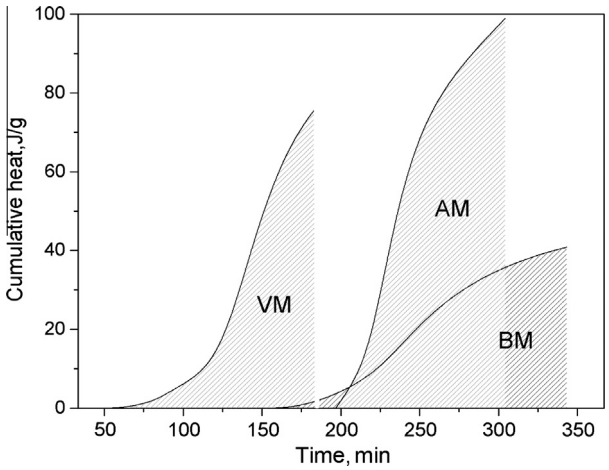

Fig. 8. Cumulative heat under C–S–H peak of alkali activated BM, AM and VM samples plotted against time.

3.4. Characterization of alkaline activated products

Fig. 6 presents the XRD patterns of SiMn slag after alkaline activation for 28 days. XRD pattern of mechanically activated VM sample prior to alkali activation has also been included in the figure. A definite change in peak characteristic was observed in the alkali activated samples. The peak identification was complicated due of overlapping of phase reflections. Most of the phases were observed in all the three types of products. The broad and diffused peak with maxima of around 30° 2θ angle in BM sample was the result of the short-range order of the C–S–A–M ($CaO–SiO_2–Al_2O_3–MgO$) glass structure from un-reacted slag [36]. The crystallinity of the alkali activation products in AM and VM increased and it is well explained by the increment of the intensity and the appearance of more X-ray peaks. This can be associated with formation of more reaction product. The main reaction product was C–S–H phases with low degree of crystallinity (JCPDS file No. 9-210 and 33-306). An analysis of XRD patterns indicated the C–S–H phases are similar to the one produced during the alkali activation of GBFS [37]. In addition, the formation of stratlingite C_2ASH_8 was observed in the hydration product of mechanically activated slag [38]. The peaks of hydrotalcite ($Mg_6Al_2CO_3(OH)_{16}\cdot 4H_2O$) and tobermorite, $(CaO, MgO)_4\cdot AH_{13}$ were identified. Peaks of calcium magnesium aluminate hydrate ($(CaO, MgO)_4\cdot Al_2O_3\cdot 13 H_2O$), some of them overlapping with hydrotalcite were also observed. Weak peaks of calcium carbonate overlapping with other phases were found.

The following images (Fig. 7) show the main morphological features of BM, AM and VM samples hydrated for 28 days. An EDS analysis of these features is summarized in Table 4. The microstructure of the BM sample was mainly comprised of discrete particles of slag, separated from each other and showing porosity (Fig. 7a). The compactness of microstructure improved in mechanically activated samples. Both AM and VM samples are characterized by compact structure and the formation of large amounts of dense gel. Calcium silicate hydrate (C–S–H, $C = CaO$, $S = SiO_2$, $H = H_2O$) gel was the principal hydration product. The morphologies of C–S–H gel have been changed with the change in CA/Si ratio. This is in agreement with early findings that the transition between C–S–H (I) and C–S–H (II) occurs at Ca/Si molar ratio 1.5 [39,40]. The nature of the gel was different in AM and VM samples. In AM, the gel phase was uniformly dispersed with partially reacted slag with Ca/Si molar ratio 1.1–1.6 (Fig. 7b). The VM has shown three distinct features, small globules type structure (Fig. 7c), dense C–S–H gel structure (Fig. 7d) and honeycomb type gel structure (Fig. 7e and f). The globular gel has shown composition close to hydrotalcite but rich in Mn content with Ca/Mn molar ratio 1.4–2.2. The honeycomb type structure with Ca/Si molar ratio 1.4–3.0 have also shown the presence on the Mn in its structure. The molar percent of Mn were found to be lesser than the globule type structure (Table 4). Similar type of honeycomb structure was observed in the 28-day hydrated samples of GBFS by other researchers [21]. By examining these structures carefully, it was found that the majority of them have grown on spherical or semi-spherical shaped morphologies. Interestingly, inspite of presence of MgO in original slag, no substitution of Ca by Mg in the C–S–H was observed in EDS results (Table 4) [41].

3.5. Mechanical properties of alkaline activated products

The results of setting time and compressive strength are summarized in Table 5. The BM samples took a long time, 390 min for initial set. A sharp decrease in setting time was observed with mechanically activated AM and VM samples. Similarly the compressive strength in BM was low which improved significantly in AM and VM. This result is also in agreement on the setting time of the samples. The compressive strength values were comparable or even better in case of VM to many reported values of alkali activated blast furnace slag or similar products [42]. Improvement in setting time and compressive strength in mechanically activated samples can be attributed to increase in compactness of microstructure and formation of different types of gel and reaction product.

3.6. Reaction structure property relation

The basic reactivity of ground SiMn slag (BM) was found to be smaller than GBFS. Mechanical activation has altered the reactivity significantly and a consequent improvement in strength was obtained. The finest particle size distribution was obtained in AM but alkali activation started earlier and strength development was much higher in VM. Thus it can be surmised that the alteration in hydration reactions was not only influenced by particle size but a combined effect of particle size (increase in surface area) and a change in reactivity (surface and bulk). It was also observed that the reactivity of particles is dependent on milling medium and device [18]. To understand the reaction behavior, the area under calorimetric peak (denotes the quantity of reaction product) of BM, AM and VM was plotted against time (Fig. 8). The ordinate denotes the cumulative heat in J/g under the calorimetric peak of different samples. Taking BM as reference, there was no major peak shift in AM but the peak intensity increased significantly. In contrast, VM has shown major shift of the peak towards the Y axis which shows that precipitation started and completed much earlier. The total area under peak was maximum in AM due to more formation of reaction products, whereas maximum strength was found in VM samples. Thus it can be anticipated that the strength development was not only influenced by the formation of more C–S–H phase, but other minor reactions and compact microstructure also contributed to it. Presence of phases such as hydrotalcite, $C_2A_SH_8$ and tobermorite, $(CaO, MgO)_4\cdot AH_{13}$ in VM further support this

observation. MnO, which was present in original SiMn slag was also found in the reaction product in VM. Thus it can be assumed that MnO has also contributed in strength development, however its role in hydration is not very clear. Based on calorimetric finding, FTIR spectra, nature of reaction products formed and mechanical properties, following order of reactivity can be proposed: VM > AM > BM.

4. Conclusions

SiMn slag of different reactivity was activated using NaOH (6 M) solution. The reactivity of slag, the reaction mechanism, hydration products formed, and their mechanical properties were studied. The following conclusions could be drawn.

1. Mechanical activation increases the reactivity of SiMn slag. The reactivity is also mill dependent. Eccentric vibratory milling produced more reactive SiMn than attrition milling.
2. The effect of mechanical activation on structural reorganization is evident from calorimetric results and FTIR spectra. The shifting of calorimetric peak in VM and occurrence of new peaks in AM and VM is associated with faster rate of reaction and acceleration of many minor reactions.
3. The main hydration product found in all samples was C–S–H gel with Mn in structure. Other hydration products were hydrotalcite, $C_2A_SH_8$, tobermorite, $(CaO, MgO)_4{\cdot}AH_{13}$. The formation of hydration products was higher in mechanically activated samples.
4. The combined effect of particle size (increase in surface area) and change in reactivity due to mechanical activation altered the alkaline activation reaction. The setting time and compressive strength development are related to the intrinsic structure developed due to enhanced reaction.
5. According to the results obtained in the current research, it is possible to suggest the possible chemical and technical viability of using SiMn slag as starting material for alkali activated cement binder.

Acknowledgements

This work has been carried out under Research Excellence Program of University of Santiago de Compostella USC-India (PEIN). The authors thank Javier Vázquez (FERROATLÁNTICA S.L.) who kindly provided the slags used in this research. We are also grateful to the Director, CSIR-National Metallurgical Laboratory, Jamshedpur (India) for his agreeable permission to publish this work.

References

[1] International Manganese Institute. <http://www.manganese.org/about_mn/production>. [accessed 22.03.13].
[2] Frias M, Sánchez de Rojas MI, Santamaría J, Rodríguez C. Recycling of silicomanganese slag as pozzolanic material in Portland cements: basic and engineering properties. Cem Concr Res 2006;36:487–91.
[3] Frias M, Sánchez de Rojas MI, Rodríguez C. The influence of SiMn slag on chemical resistance of blended cement pastes. Constr Build Mater 2009;23:1472–5.
[4] Zhang X, Ni W, Wu J, Zhu L. Hydration mechanism of a cementitious material prepared with Si–Mn slag. Int J Miner Metall Mater 2011;18:234–9.
[5] García-Triñanes P, Pereiro G, Bao M. Optimization of the alkaline activation process of difficult-to-treat inorganic wastes. In: Proceedings of 13th international congress on chemistry of cement. Madrid; 2011. p. 1–7.
[6] Shi C, Krivenko PV, Roy DM. Alkali-activated cements and concretes. Abingdon UK: Taylor and Francis; 2006.
[7] Purdon AO. The action of alkalis on blast furnace slag. J Soc Chem Ind 1940;59:191–202.
[8] Roy DM. Alkali-activated cements – opportunities and challenges. Cem Concr Res 1999;29:249–54.
[9] Wang SD, Pu XC, Scrivener KL, Pratt PL. Alkali-activated slag cement and concrete: a review of properties and problems. Adv Cem Res 1995;7:93–102.
[10] Richardson IG, Brough AR, Groves GW, Dobson CM. The characterization of hardened alkali-activated blast-furnace slag pastes and the nature of the calcium silicate hydrate (C–S–H) paste. Cem Concr Res 1994;24:813–29.
[11] Wang SD, Scrivener KL. ^{29}Si and ^{27}Al NMR study of alkali-activated slag. Cem Concr Res 2003;33:769–74.
[12] Fernández-Jiménez A, Puertas F, Arteaga A. Determination of kinetic equations of alkaline activation of blast furnace slag by means of calorimetric data. J Therm Anal Calorim 1998;52:945–55.
[13] Fernández-Jiménez A, Puertas F. Alkali-activated slag cements: kinetic studies. Cem Concr Res 1997;27:359–68.
[14] Juhasz AJ, Opoczky L. Mechanical activation of minerals by grinding: pulverizing and morphology of particles. Chichester UK: Ellis Horwood Limited; 1994.
[15] Boldyrev VV. Mechanochemistry and mechanical activation of solids. Russ Chem Rev 2006;75:177–89.
[16] Balaz P. Mechanochemistry in nanoscience and minerals engineering. Verlag – Berlin – Heidelberg: Springer; 2008.
[17] Kumar S, Kumar R, Alex TC, Bandopadhyay A, Mehrotra SP. Effect of mechanically activated fly ash on the properties of geopolymer cement. In: Davidovits J, editor. Proceedings of Geopolymer Congress. France; 2005. p. 113–6.
[18] Kumar S, Kumar R, Alex TC, Bandopadhyay A, Mehrotra SP. Influence of reactivity of fly ash on geopolymerisation. Adv Appl Ceram 2007;106:120–7.
[19] Kumar S, Kumar R, Bandopadhyay A, Alex TC, RaviKumar B, Das SK, et al. Mechanical activation of granulated blast furnace slag and its effect on the properties and structure of portland slag cement. Cem Concr Compos 2008;30:679–85.
[20] Temuujin J, Williams RP, Riessen AV. Effect of mechanical activation of fly ash on the properties of geopolymer cured at ambient temperature. J Mater Process Technol 2009;209:5276–80.
[21] Kumar R, Kumar S, Badjena S, Mehrotra SP. Hydration of mechanically activated granulated blast furnace slag. Met Trans B 2005;36:873–83.
[22] Kumar S, Kumar R. Mechanical activation of fly ash: effect on reaction, structure and properties of resulting geopolymer. Ceram Int 2011;37:533–41.
[23] Kolb G, Ott K. Efficient agitator bead mills. Eur Coal 1992;4:199–214.
[24] Kapur PC, Healy TW, Scales PJ, Boger DV, Wilson D. Role of dispersants in kinetics and energetics of stirred ball mill grinding. Int J Miner Process 1996;47:141–52.
[25] Bernhardt P. Investigations into process dynamics and control of a laboratory agitator bead mill. Intl J Miner Proces 1996;44–45:629–40.
[26] Berthiaux H, Heitzmann D, Dodds JA. Validation of a model of a stirred bead mill by comparing results obtained in batch and continuous mode grinding. Intl J Miner Proces 1996;44–45:653–61.
[27] Gock E, Beenken W, Gruschka M. Eccentric vibrating mill. US Patent 5570848. 5 November; 1996.
[28] Gock E, Kurrer KE. Eccentric vibratory mills: theory and practice. Powder Technol 1999;105:302–10.
[29] IS 4031. Method of physical test of hydraulic cement. Bureau of Indian Standard; 1996.
[30] Bernal A, Provis JL, Volker R, de-Guitiérrez RM. Evolution of binder structure in sodium silicate-activated slag-metakaolin blends. Cem Concr Compos 2011;33:46–54.
[31] Yu P, Kirkpatrick RJ, Poe B, McMillan PF, Cong X. Structure of calcium silicate hydrate (C–S–H): near-, mid-, and far-infrared spectroscopy. J Am Ceram Soc 1999;82:742–8.
[32] Huang CK, Kerr PF. Infrared study of the carbonate minerals. Am Mineral 1960;45:311–24.
[33] Yip CK, Lukey GC, Provis JL, Van-Deventer JSJ. Carbonate mineral addition to metakaolin-based geopolymers. Cem Concr Compos 2008;30:979–85.
[34] Farmer VC. The infrared spectra of minerals. Great Britain: Mineralogical Society Monograph; 1974.
[35] Gadsden JA. Infrared spectra of minerals and related inorganic compounds. USA: Butterworths; 1975.
[36] Song S, Jennings HM. Pore solution chemistry of alkali-activated ground granulated blast-furnace slag. Cem Concr Res 1999;29:159–70.
[37] Li C, Sun H, Li L. The comparison between alkali-activated slag (Si + Ca) and metakaolin (Si + Al) cements. Cem Concr Res 2010;40:1341–9.
[38] Provis J, Van-Deventer JSJ. Geopolymers: structure, processing, properties and industrial applications. UK: Woodhead Publishing Limited; 2009.
[39] Taylor HFW. Cement chemistry. 2nd ed.. London: Thomas Telford; 1997.
[40] Thomas JJ, Jennings HGM. A colloidal interpretation of chemical aging of the C–S–H gel and its effects on the properties of cement paste. Cem Concr Res 2006;36:30–8.
[41] Ben Haha M, Lothenbach B, LeSaout G, Winnefeld F. Influence of slag chemistry on the hydration of alkali-activated blast-furnace slag—Part I: Effect of MgO. Cem Concr Res 2011;41:955–63.
[42] Kumar S, Kumar R, Mehrotra SP. Influence of granulated blast furnace slag on the reaction, structure and properties of fly ash based geopolymer. J Mater Sci 2010;45:607–15.